

VO₂-Based Switchable Metasurface With Broadband Photonic Spin Hall Effect and Absorption

Zhao Xu and Zhengyong Song ^{ID}

Abstract—Arbitrary control and dynamic tuning of circularly polarized (CP) wave are of great significance to photonic research and application. Here, a terahertz switchable metasurface is designed with bifunctional properties based on a mixed structure of graphene and vanadium dioxide (VO₂). The design consists of VO₂ strips, topas spacer, VO₂ film, graphene patch, topas spacer, and metallic film. When VO₂ is metal, this metasurface realizes photonic spin Hall effect (PSHE) for CP wave in a wide frequency band of 0.7–1.5 THz. When VO₂ is insulator, the design behaves as an absorber. It has a broadband absorption with more than 90% absorptance in the range of 0.48–1.88 THz, and there are two resonant peaks with ~100% absorptance at 0.92 THz and 1.74 THz. Meanwhile, absorption bandwidth and intensity can be dynamically tuned by changing Fermi energy level of graphene. Besides, broadband absorption is robust against incident angle. Our design may promote the realization of terahertz switchable and multifunctional metasurfaces.

Index Terms—Absorption, graphene, photonic spin Hall effect, terahertz, VO₂.

I. INTRODUCTION

TADITIONAL methods of manipulating electromagnetic wave depend on gradually changing the phase during propagation, so the involved devices have complex and irregular shapes. It is not in line with the current trend of integration. In recent years, metasurface as a 2D ultra-thin metamaterial integrates artificially subwavelength microstructure into an interface. Since the concept was put forward, metasurface has attracted much attention because of its extraordinary electromagnetic properties [1]–[3]. In addition, metasurface with the subwavelength thickness can modify boundary conditions of incident waves to control amplitude, phase, polarization, and waveform. Therefore, many interesting phenomena have been proposed, such as beam-steerers [4]–[6], photonic spin Hall effects (PSHEs) [7]–[9], focusing lenses [10]–[12], optical holograms [13]–[15], intelligent codings [16]–[18], waveplates [19]–[21], invisible cloaks [22]–[24], and so on.

Arbitrary control of circularly polarized (CP) wave has always been of great significance to photonic research and application.

Manuscript received June 11, 2021; revised July 15, 2021; accepted July 16, 2021. Date of publication July 21, 2021; date of current version August 6, 2021. This work was supported in part by National Natural Science Foundation of China under Grant 11974294, and in part by the Guangdong Basic and Applied Basic Research Foundation under Grant 2020A1515010375. (Corresponding author: Zhengyong Song.)

The authors are with the Institute of Electromagnetics and Acoustics, Xiamen University, Xiamen 361005, China, and also with the Shenzhen Research Institute of Xiamen University, Shenzhen 518057, China (e-mail: 34320201150188@stu.xmu.edu.cn).

Digital Object Identifier 10.1109/JPHOT.2021.3098534

The recently proposed Pancharatnam-Berry (PB) metasurfaces show unprecedented abilities to control CP wave. Phase response in this system is determined by the orientation (not the shape) of meta-atoms. The design and manufacture of this metasurface are relatively easy. Besides, PB metasurfaces can show spin-dependent and dispersion-free phase distribution. This extraordinary characteristic makes PB metasurfaces widely used in various aspects, including optical sensing [25], [26], biomolecule detection [27], [28], and communication technology [29], [30]. But previous designs mainly focus on the realization of single function of CP wave.

Dynamic tunability has always been the goal of metasurface. In recent years, the development of two-dimensional materials provides a new prospect for the active control of electromagnetic waves [31], [32]. Graphene, a novel material with carbon atoms densely packed into a single-layer honeycomb lattice structure, is a good candidate to meet the requirement of adjustability. It has excellent physical properties such as monatomic thickness and optical transparency [33], [34]. Fermi energy level of graphene can be moved by electrostatic gating, so that amplitude and phase responses of electromagnetic waves can be dynamically tuned [35], [36]. With the development of high-level graphene film synthesis technology [37], graphene has been applied as absorber in experiments. In 2017, Yi et al. proposed a transparent absorber with the patterned graphene, which has a peak absorption close to 100% and a wide bandwidth of 3 GHz [38]. In 2019, Lu et al. realized a transparent microwave absorber based on patterned graphene, which has an absorption rate of >90% over 5–16 THz. And its thickness is only 1/13 wavelength [39]. All these efforts open up exciting possibilities for designing tunable metasurfaces.

Recently, phase change materials have been proposed and widely used in various fields. Vanadium dioxide (VO₂) as one of phase change materials undergoes a structural transformation from monoclinic phase to tetragonal phase at ~340 K [40], [41]. This phase transformation can be caused by light excitation, thermal excitation or external electric excitation. After phase transition, the conductivity of VO₂ changes significantly by several orders of magnitude, which can be employed to control photoelectric properties of related materials. Therefore, VO₂ is very attractive for adjustable and switchable devices. Some VO₂-based tunable devices have also been proposed. In 2015, Kocer et al. proposed a nanostructured thermal absorber with the mixed structure of gold and VO₂. When the sample is heated, absorptance can change from 20% to 90% [42]. In 2019, Lei et al. realized a dynamic absorber based on VO₂ structure in

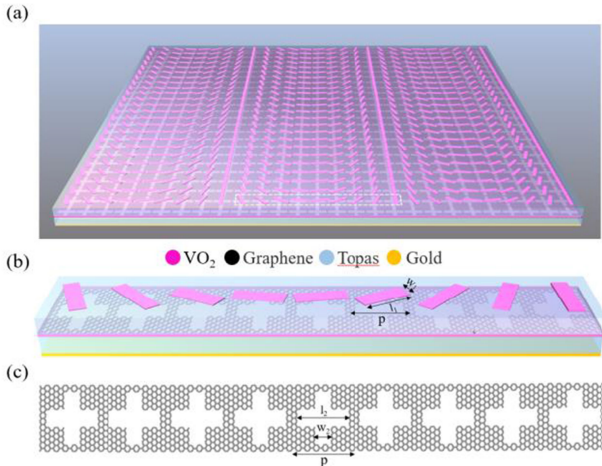


Fig. 1. (a) 3D schematic diagram of the proposed bifunctional metasurface. A super-cell is surrounded by a dotted line. (b) 3D schematic diagram of a super-cell and (c) top view of graphene film. Here, $l_1 = 90 \mu\text{m}$, $w_1 = 12 \mu\text{m}$, $l_2 = 90 \mu\text{m}$, $w_2 = 16 \mu\text{m}$ and $p = 97.5 \mu\text{m}$.

infrared band. When VO₂ changes from the insulating state to the metallic state, 90% absorption bandwidth changes from 3069 nm to 632 nm [43]. The dynamic adjustment of absorption bandwidth is realized.

In this work, we combine graphene and VO₂ to present a broadband bifunctional metasurface. When VO₂ is metal, the designed metasurface can realize broadband PSHE. When VO₂ is insulator, the designed metasurface can realize broadband absorption. Bandwidth and efficiency of absorption can be dynamically adjusted by applying different Fermi energy levels.

II. DESIGN AND MODEL

A 3D schematic diagram of the designed metasurface is shown in Fig. 1. It consists of six layers from top to bottom: VO₂ strips, upper topas ($\epsilon_r = 2.35$) spacer, VO₂ film, graphene layer, lower topas spacer, and a metallic ground layer. The thicknesses of VO₂ strips, VO₂ film, and the bottom metallic substrate are 1 μm . The lower topas thickness is 41 μm , and the upper topas thickness is 40 μm . The period of unit cell is 97.5 μm . The frequency-dependent complex dielectric permittivity of VO₂ is described by Drude model $\epsilon(w) = \epsilon_\infty - \frac{w_p^2}{w^2 + i\gamma w}$ in the terahertz range [44], [45]. In our simulation, dielectric permittivity ϵ_∞ is 12 and collision frequency γ is 5.75×10^{13} rad/s. Plasma frequency w_p is 1.14×10^{15} rad/s (3.62×10^{13} rad/s) for the metallic (insulating) state. The temperature of VO₂ can be adjusted by optical pumping. Graphene layer is modeled as an infinitesimal thin resistive surface, and the conductivity of graphene can be expressed by Kubo formula [46], [47].

$$\begin{aligned} \sigma(\omega, E_F, \tau, T) &= \sigma_{\text{intra}}(\omega, E_F, \tau, T) \\ &\quad + \sigma_{\text{inter}}(\omega, E_F, \tau, T) \\ &= \frac{2ie^2k_B T}{\pi\hbar^2(\omega + i\tau^{-1})} \ln \left[2 \cosh \left(\frac{E_F}{2k_B T} \right) \right] \\ &\quad + \frac{e^2}{4\hbar} \left[\frac{1}{2} + \frac{1}{\pi} \arctan \left(\frac{\hbar\omega - 2E_F}{2k_B T} \right) \right] \end{aligned}$$

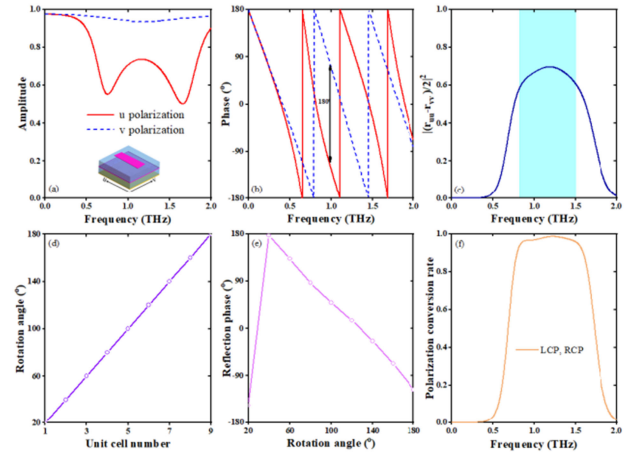


Fig. 2. Reflection amplitude (a) and reflection phase (b) under u-polarized and v-polarized waves. (c) Efficiency of anomalous mode. The shaded area indicates the working bandwidth defined by the efficiency $|r_{uu} - r_{vv}|/2 > 0.6$. (d) The designed super-cell is composed of nine units whose VO₂ strips rotate 20° in turn. (e) Reflection phase of cross-polarized reflected wave as a function of rotation angle. (f) Polarization conversion rate under CP wave incidence.

$$-\frac{i}{2\pi} \ln \frac{(\hbar\omega + 2E_F)^2}{(\hbar\omega - 2E_F)^2 + (2k_B T)^2}$$

Herein, the initial Fermi energy levels of graphene are $E_F = 0.8 \text{ eV}$. The used relaxation time is $\tau = 0.1 \text{ ps}$.

III. RESULTS AND DISCUSSIONS

A. The Designed Switchable Metasurface Achieves PSHE When VO₂ Strip and VO₂ Film are Metal

Spin Hall effect (SHE) is a physical phenomenon related to the spin-dependent trajectory of current caused by spin-orbit interaction [48], [49]. PSHE is a photon analogy of SHE, and it refers to the transverse spin splitting of optical orbit. Through the interaction of photon spin angular momentum and orbital angular momentum, transverse splitting of optical orbit originates from the opposite geometric phases of two spins/polarizations [50], [51]. PB metasurface is an ideal tool for manipulating circular polarization. Based on rigorous Jones matrix analysis, a general criterion to design metasurfaces that can realize efficient PSHE is established. When meta-atom rotates by φ , anomalous reflection will carry an additional PB phase of 2φ . Due to the existence of metal substrate, the designed system is totally reflective. When VO₂ is metal, VO₂ strip, topas spacer, and VO₂ film constitute a reflective system. Its transmission channel is strictly terminated, which is beneficial to concentrate energy and improve working efficiency. According to Jones matrix analysis, theoretical criterion of PB meta-atom meeting 100% efficiency is $|r_{uu}| = |r_{vv}| = 1$ and $r_{uu} + r_{vv} = 0$, where u and v denote two main axes of PB meta-atom. The criterion becomes $\theta_{uu} - \theta_{vv} = \pi$, indicating that the desired system is a perfect half waveplate working in the reflective mode. On this basis, the designed unit cell is optimized to make phase difference $\theta_{uu} - \theta_{vv}$ stabilized at $\sim\pi$ within a wide band. Fig. 2(a) and 2(b) depicts reflection amplitude and phase of

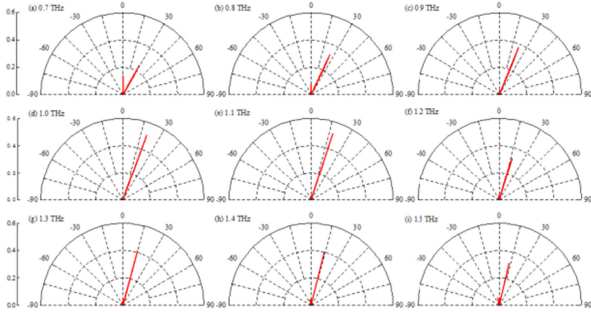


Fig. 3. Normalized far-field power radiation pattern when LCP waves with different frequencies are incident from 0°. At 0.7, 0.8, 0.9, 1.0, 1.1, 1.2, 1.3, 1.4, 1.5 THz, anomalous reflection angle is 29.2°, 25.3°, 22.3°, 20°, 18.1°, 16.6°, 15.3°, 14.2°, 13.2°, respectively.

the proposed meta-atom excited by linearly polarized wave. Reflection amplitudes of unit cell along two main axes are above 70% at 1.0 THz, and two resonances in u direction are mainly caused by plasmonic resonances between VO₂ strip and VO₂ film. The calculated results show an equivalent behavior of a half-wave plate in a wide frequency band of 0.84-1.51 THz. As shown in Fig. 2(c), reflection efficiency of PB atom is calculated by $|(\mathbf{r}_{uu} - \mathbf{r}_{vv})/2|^2$. It is found that the absolute efficiency exceeds 60% in the working frequency band, and the loss is mainly caused by metallic behavior of VO₂ in terahertz band. In Fig. 2(d), VO₂ strips are rotated by 20° in turn, and nine unit cells as a super-cell to cover π phase. Fig. 2(e) shows reflection phase of cross-polarized reflected wave as a function of rotation angle. According to PB phase theory, when rotation angle is 20°, the corresponding phase changes by 40°. Therefore, an efficient PSHE can be realized. In Fig. 2(f), polarization conversion rate ($PCR = \frac{|r_{LCP}/RCP|^2}{|r_{LCP}|^2 + |r_{RCP}|^2}$) is calculated. It is found that the value of PCR is greater than 90% in the working frequency range of 0.79-1.59 THz, which realizes high-efficiency polarization conversion.

Periodic super-cells are constructed to achieve PSHE within a wide frequency band. According to the generalized Snell's law, as the impinging CP wave strikes PB metasurface, anomalous reflection angle θ_r is determined by $\sin(\theta_r) = \sin(\theta_i) + \frac{\xi_x}{k_0}$, where θ_i denotes incident angle, k_0 is the free-space wavevector, and $\xi_x = \pm \frac{2\varphi}{p}$ is the spin-dependent wavevector. Rotation angle φ between adjacent VO₂ bars in the x direction is 20° so as to form a phase gradient. When CP wave is incident from the vertical direction, anomalous reflection angle θ_r will be 20° at 1 THz. CP beams with opposite chirality will be deflected from $\pm 29.2^\circ$ to $\pm 13.2^\circ$ in the frequency range of 0.7-1.5 THz. Fig. 3 depicts the normalized far-field power radiation pattern of left-handed CP (LCP) wave. When incident frequency is 0.7 THz under normal incidence, the reflected wave is abnormally deflected to 29.2°. With the increase of incident frequency, reflection angle begins to decrease. When incident frequency is 1.5 THz, deflected angle is 13.2°. In the interesting frequency range, reflection intensity ($|\mathbf{E}|^2$) is as high as 51%, and the loss is mainly due to VO₂ absorption. Fig. 4 shows the normalized power pattern of right-handed CP (RCP) wave. Obviously, incident RCP beams are abnormally deflected to

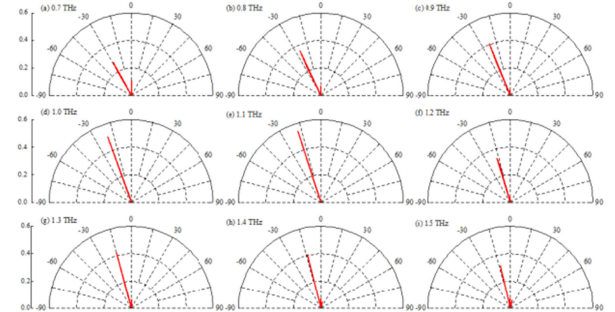


Fig. 4. Normalized far-field power radiation pattern when RCP waves with different frequencies are incident from 0°. At 0.7, 0.8, 0.9, 1.0, 1.1, 1.2, 1.3, 1.4, 1.5 THz, anomalous reflection angle is -29.2°, -25.3°, -22.3°, -20°, -18.1°, -16.6°, -15.3°, -14.2°, -13.2°, respectively.

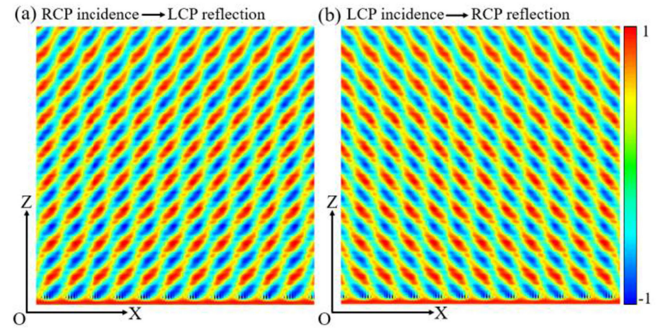


Fig. 5. Simulated E_y -field patterns under the illumination of LCP (a) and RCP (b) waves at 1.0 THz in the xoz plane.

opposite directions, which is the chiral feature of PSHE. This is mainly because electric field direction and gradient direction are opposite. Therefore, our metasurface can realize CP beam control in a wide band range.

According to the generalized Snell's law, this gradient metasurface should exhibit anomalous reflection at the angle of $\theta_r = 20^\circ$ when the frequency of incident wave is 1.0 THz. To further verify the prediction, 3D full-wave numerical simulations are performed. Fig. 5 displays the reflected E_y -field for RCP (Fig. 5(a)) and LCP (Fig. 5(b)) incident waves, and it shows well-defined wavefronts. It is easy to see how two CP waves are deflected to opposite sides of surface normal.

B. The Designed Switchable Metasurface Achieves Broadband Absorption When VO₂ Strip and VO₂ Film are Insulator

We introduce graphene layer and add cross pattern to increase absorption. The bottom metal substrate is added to realize zero transmission. Absorptance $A(w)$ of the proposed metasurface can be calculated by $A(w) = 1 - |r(w)|^2 - |t(w)|^2 \approx 1 - |r(w)|^2$, where $r(w)$ and $t(w)$ are reflection and transmission coefficients. If impedance of the designed metasurface matches that of free space, wave reflection will be eliminated, thus near-unity absorption can be achieved. Fig. 6 shows absorptance spectra when different Fermi energy levels are applied to graphene. When Fermi energy level is increasing, metasurface exhibits broadband adjustable absorption. It can be found that at different Fermi energy levels, there are two obvious absorption

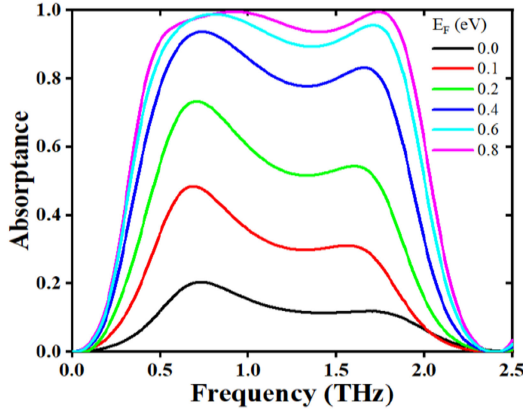


Fig. 6. Broadband absorption of CP wave at different Fermi energy levels of graphene.

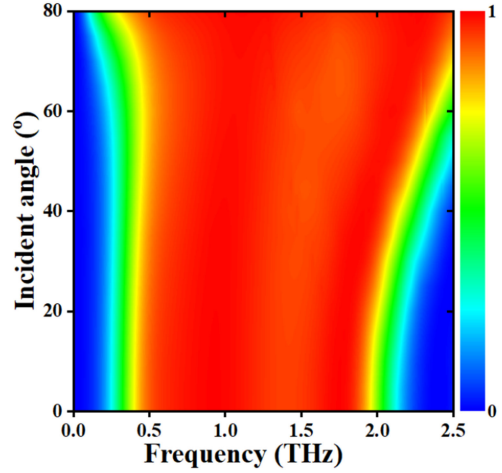


Fig. 8. Absorptance of the proposed structure as a function of frequency and incident angle for CP wave.

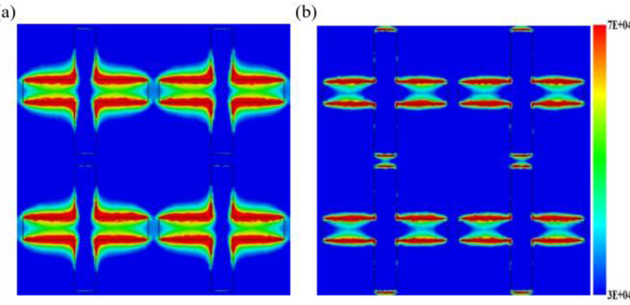


Fig. 7. Electric field ($|E|$) distributions in the graphene patch plane at 0.92 THz (a) and 1.74 THz (b).

peaks around 0.92 THz and 1.74 THz. Absorptance at two absorption peaks almost reaches 100% when Fermi energy level is 0.8 eV. With the increase of Fermi energy level, absorption intensity gradually increases. Dynamic tuning of absorptance is realized from 11% to 100% at the frequency of 1.74 THz.

In order to elucidate physical mechanism of broadband absorption in the designed system, electric field distributions of broadband absorption are calculated. Figs 7(a) and 7(b) show the top view of simulated electric field distribution of broadband absorber in the XOY plane at two absorption peaks. Electric field is strongly enhanced in the gap between two graphene squares at 0.92 THz. Electric field is confined around the edge of a single graphene square at 1.74 THz, and the intensity of electric field in the gap between two graphene squares is obviously reduced. Therefore, low-frequency resonance in broadband absorption is mainly caused by the coupling interaction between graphene squares, while high-frequency resonance in broadband absorption is caused by the fundamental resonance mode of a single graphene square. The combination of these two resonances ensures broadband performance of the designed absorber.

To make the designed broadband absorber valuable in potential applications, the performance of broadband absorber is expected to be stable with the change of incident angle. Therefore, we further verify the sensitivity of the designed device to oblique incidence. The angle between incident wavevector and normal (0°) is defined as incident angle. As shown in Fig. 8, when incident angle changes from 0° to 80° , absorption intensity and

bandwidth are relatively stable within 50° . With the increase of incident angle, bandwidth range tends to increase. Thus, the device we designed has good insensitivity to incident angle.

IV. CONCLUSION

To summarize, a switchable metasurface with bifunctional properties is proposed based on graphene and VO_2 . When VO_2 is metal, the designed metasurface owns phase difference of 180° in a wide frequency band of 0.7–1.5 THz under normal incidence of two orthogonal linear polarized waves, and reflection efficiency is more than 60%. The design can realize broadband beam control of CP. When VO_2 is insulator, the designed metasurface can realize broadband absorption. Its absorptance is more than 90% in the frequency range of 0.48–1.88 THz. Low-frequency absorption peak is mainly caused by the coupling between graphene patches, while high-frequency absorption peak is caused by electric dipole resonance of individual graphene patch. Besides, absorption bandwidth and intensity can be dynamically adjusted by applying different Fermi energy levels. Our findings may stimulate the development of switchable and multifunctional devices [52]–[55].

REFERENCES

- [1] M. Tymchenko, J. S. Gomez-Diaz, J. Lee, N. Nookala, M. A. Belkin, and A. Alu, "Gradient nonlinear pancharatnam-berry metasurfaces," *Phys. Rev. Lett.*, vol. 115, no. 20, Nov. 2015, Art. no. 207403.
- [2] H. T. Chen, A. J. Taylor, and N. Yu, "A review of metasurfaces: Physics and applications," *Reports Prog. Phys.*, vol. 79, no. 7, Jun. 2016, Art. no. 076401.
- [3] S. Sun, Q. He, J. Hao, S. Xiao, and L. Zhou, "Electromagnetic metasurfaces: Physics and applications," *Adv. Opt. Photon.*, vol. 11, no. 2, pp. 380–479, Jun. 2019.
- [4] X. Ni, N. K. Emani, A. V. Kildishev, A. Boltasseva, and V. M. Shalaev, "Broadband light bending with plasmonic nanoantennas," *Science*, vol. 335, no. 6067, pp. 427–427, Jan. 2012.
- [5] C. Pfeiffer and A. Grbic, "Metamaterial huygens' surfaces: Tailoring wave fronts with reflectionless sheets," *Phys. Rev. Lett.*, vol. 110, no. 19, May 2013, Art. no. 197401.
- [6] W. Luo, S. Xiao, Q. He, S. Sun, and L. Zhou, "Photonic spin hall effect with nearly 100% efficiency," *Adv. Opt. Mater.*, vol. 3, no. 8, pp. 1102–1108, Aug. 2015.

- [7] W. Luo, S. Sun, H. X. Xu, Q. He, and L. Zhou, "Transmissive ultrathin pancharatnam-berry metasurfaces with nearly 100% efficiency," *Phys. Rev. Appl.*, vol. 7, no. 4, Apr. 2017, Art. no. 044033.
- [8] O. Hosten and P. Kwiat, "Observation of the spin hall effect of light via weak measurements," *Science*, vol. 319, no. 5864, pp. 787–790, Feb. 2008.
- [9] F. Aieta *et al.*, "Aberration-free ultrathin flat lenses and axicons at telecom wavelengths based on plasmonic metasurfaces," *Nano Lett.*, vol. 12, no. 9, pp. 4932–4936, Sep. 2012.
- [10] X. Li, S. Xiao, B. Cai, Q. He, T. Cui, and L. Zhou, "Flat metasurfaces to focus electromagnetic waves in reflection geometry," *Opt. Lett.*, vol. 37, no. 23, pp. 4940–4942, Dec. 2012.
- [11] A. Pors, M. G. Nielsen, R. L. Eriksen, and S. I. Bozhevolnyi, "Broadband focusing flat mirrors based on plasmonic gradient metasurfaces," *Nano Lett.*, vol. 13, no. 2, pp. 829–834, Feb. 2013.
- [12] P. Genevet and F. Capasso, "Holographic optical metasurfaces: A review of current progress," *Reports Prog. Phys.*, vol. 78, no. 2, Feb. 2015, Art. no. 024401.
- [13] G. Zheng, H. Muhlenbernd, M. Kenney, G. Li, T. Zentgraf, and S. Zhang, "Metasurface holograms reaching 80% efficiency," *Nature Nanotechnol.*, vol. 10, no. 4, pp. 308–312, Apr. 2015.
- [14] W. T. Chen *et al.*, "High-efficiency broadband meta-hologram with polarization-controlled dual images," *Nano Lett.*, vol. 14, no. 1, pp. 225–230, Jan. 2014.
- [15] L. Huang *et al.*, "Three-dimensional optical holography using a plasmonic metasurface," *Nat. Commun.*, vol. 4, no. 1, Nov. 2013, Art. no. 2808.
- [16] T. Cui, M. Qi, X. Wan, J. Zhao, and Q. Cheng, "Coding metamaterials, digital metamaterials and programmable metamaterials," *Light-Sci. Appl.*, vol. 3, Oct. 2014, Art. no. e218.
- [17] S. Liu *et al.*, "Anisotropic coding metamaterials and their powerful manipulation of differently polarized terahertz waves," *Light-Sci. Appl.*, vol. 5, May 2016, Art. no. 16076.
- [18] A. Pors, F. Ding, Y. Chen, I. R. Radko, and S. I. Bozhevolnyi, "Random-phase metasurfaces at optical wavelengths," *Sci. Rep.*, vol. 6, Jun. 2016, Art. no. 28448.
- [19] A. Pors, M. G. Nielsen, and S. I. Bozhevolnyi, "Broadband plasmonic half-wave plates in reflection," *Opt. Lett.*, vol. 38, no. 4, pp. 513–515, Feb. 2013.
- [20] Z. Song, J. Zhu, C. Zhu, Z. Yu, and Q. H. Liu, "Broadband cross polarization converter with unity efficiency for terahertz waves based on anisotropic dielectric meta-reflectarrays," *Mater. Lett.*, vol. 159, pp. 269–272, Nov. 2015.
- [21] F. Ding, Z. Wang, S. He, V. M. Shalaev, and A. V. Kildishev, "Broadband high-efficiency half-wave plate: A supercell-based plasmonic metasurface approach," *ACS Nano*, vol. 9, no. 4, pp. 4111–4119, Apr. 2015.
- [22] X. Ni, Z. J. Wong, M. Mrejen, Y. Wang, and X. Zhang, "An ultrathin invisibility skin cloak for visible light," *Science*, vol. 349, no. 6254, pp. 1310–1314, Sep. 2015.
- [23] H. Chu *et al.*, "A hybrid invisibility cloak based on integration of transparent metasurfaces and zero-index materials," *Light-Sci. Appl.*, vol. 7, pp. 50, Aug. 2018.
- [24] H. Xu *et al.*, "Deterministic approach to achieve broadband polarization-independent diffusive scatterings based on metasurfaces," *ACS Photon.*, vol. 5, no. 5, pp. 1691–1702, May 2018.
- [25] Y. Yang, R. C. Costa, M. J. Fuchter, and A. J. Campbell, "Circularly polarized light detection by a chiral organic semiconductor transistor," *Nature Photon.*, vol. 7, no. 8, pp. 634–638, Aug. 2013.
- [26] S. Yoo and Q. Park, "Metamaterials and chiral sensing: A review of fundamentals and applications," *Nano Photon.*, vol. 8, no. 2, pp. 249–261, Feb. 2019.
- [27] B. L. Feringa, "In control of motion: From molecular switches to molecular motors," *Acc. Chem. Res.*, vol. 34, no. 6, pp. 504–513, Jun. 2001.
- [28] E. Hendry *et al.*, "Ultrasensitive detection and characterization of biomolecules using superchiral fields," *Nature Nanotechnol.*, vol. 5, no. 11, pp. 783–787, Nov. 2010.
- [29] J. Wang *et al.*, "Terabit free-space data transmission employing orbital angular momentum multiplexing," *Nature Photon.*, vol. 6, no. 7, pp. 488–496, Jul. 2012.
- [30] N. Bozinovic *et al.*, "Terabit-scale orbital angular momentum mode division multiplexing in fibers," *Science*, vol. 340, no. 6140, pp. 1545–1548, Jun. 2013.
- [31] S. Zeng *et al.*, "Graphene-gold metasurface architectures for ultrasensitive plasmonic biosensing," *Adv. Mater.*, vol. 27, no. 40, pp. 6163–6169, Oct. 2015.
- [32] S. F. Shi *et al.*, "Optimizing broadband terahertz modulation with hybrid graphene/metasurface structures," *Nano Lett.*, vol. 15, no. 1, pp. 372–377, Jan. 2007.
- [33] O. Balci, E. O. Polat, N. Kakenov, and C. Kocabas, "Graphene-enabled electrically switchable radar-absorbing surfaces," *Nature Commun.*, vol. 6, Mar. 2015, Art. no. 6628.
- [34] A. H. C. Neto, F. Guinea, N. M. R. Peres, K. S. Novoselov, and A. K. Geim, "The electronic properties of graphene," *Rev. Mod. Phys.*, vol. 81, no. 1, pp. 109–162, Jan. 2009.
- [35] J. Zhang, X. Wei, M. Premaratne, and W. Zhu, "Experimental demonstration of an electrically tunable broadband coherent perfect absorber based on a graphene-electrolyte-graphene sandwich structure," *Photon. Res.*, vol. 7, no. 8, pp. 868–874, Aug. 2019.
- [36] J. Zhang *et al.*, "Dynamic scattering steering with graphene-based coding metamirror," *Adv. Opt. Mater.*, vol. 8, no. 19, Oct. 2020, Art. no. 2000683.
- [37] L. Sun *et al.*, "A force-engineered lint roller for superclean graphene," *Adv. Mater.*, vol. 31, no. 43, Oct. 2019, Art. no. 1902978.
- [38] D. Yi, X. C. Wei, and Y. L. Xu, "Transparent microwave absorber based on patterned graphene: Design, measurement, and enhancement," *IEEE Trans. Nanotechnol.*, vol. 16, no. 3, pp. 484–490, May 2017.
- [39] W. B. Lu *et al.*, "Flexible and optically transparent microwave absorber with wide bandwidth based on graphene," *Carbon*, vol. 152, pp. 70–76, Nov. 2019.
- [40] M. J. Dicken *et al.*, "Frequency tunable near-infrared metamaterials based on VO₂ phase transition," *Opt. Exp.*, vol. 17, no. 20, pp. 18330–18339, Sep. 2009.
- [41] M. A. Kats *et al.*, "Ultra-thin perfect absorber employing a tunable phase change material," *Appl. Phys. Lett.*, vol. 101, no. 22, Nov. 2012, Art. no. 221101.
- [42] H. Kocer *et al.*, "Thermal tuning of infrared resonant absorbers based on hybrid gold-VO₂ nanostructures," *Appl. Phys. Lett.*, vol. 106, no. 16, Apr. 2015, Art. no. 161104.
- [43] L. Lei, F. Lou, K. Tao, H. Huang, X. Cheng, and P. Xu, "Tunable and scalable broadband metamaterial absorber involving VO₂-based phase transition," *Photon. Res.*, vol. 7, no. 7, pp. 734–741, Jul. 2019.
- [44] Y. Zhu, Y. Zhao, M. Holtz, Z. Fan, and A. A. Bernussi, "Effect of substrate orientation on terahertz optical transmission through VO₂ thin films and application to functional antireflection coatings," *J. Opt. Soc. Amer. B*, vol. 29, no. 9, pp. 2373–2378, Sep. 2012.
- [45] S. Wang, L. Kang, and D. H. Werner, "Hybrid resonators and highly tunable terahertz metamaterials enabled by vanadium dioxide (VO₂)," *Sci. Rep.*, vol. 7, Jun. 2017, Art. no. 4326.
- [46] G. W. Hanson, "Dyadic green's functions and guided surface waves for a surface conductivity model of graphene," *J. Appl. Phys.*, vol. 103, no. 6, Mar. 2008, Art. no. 064302.
- [47] M. Jablan, H. Buljan, and M. Soljacic, "Plasmonics in graphene at infrared frequencies," *Phys. Rev. B*, vol. 80, no. 24, Dec. 2009, Art. no. 245435.
- [48] J. E. Hirsch, "Spin hall effect," *Phys. Rev. Lett.*, vol. 83, no. 9, pp. 1834–1837, Aug. 1999.
- [49] K. Y. Bliokh, F. J. Rodriguez-Fortuno, F. Nori, and A. V. Zayats, "Spin-orbit interactions of light," *Nature Photon.*, vol. 9, no. 12, pp. 796–808, Dec. 2015.
- [50] X. Yin, Z. Ye, J. S. Rho, Y. Wang, and X. Zhang, "Photonic spin hall effect at metasurfaces," *Science*, vol. 339, no. 6126, pp. 1405–1407, Mar. 2013.
- [51] S. Xiao, J. Wang, F. Liu, S. Zhang, X. Yin, and J. Li, "Spin-dependent optics with metasurfaces," *Nano Photon.*, vol. 6, no. 1, pp. 215–234, Jan. 2017.
- [52] Z. Jiang *et al.*, "Broadband and wide field-of-view plasmonic metasurface-enabled waveplates," *Sci. Rep.*, vol. 4, Dec. 2014, Art. no. 7511.
- [53] S. Jiang *et al.*, "Controlling the polarization state of light with a dispersion-free metastructure," *Phys. Rev. X*, vol. 4, no. 2, May 2014, Art. no. 021026.
- [54] F. Ding, S. Zhong, and S. I. Bozhevolnyi, "Vanadium dioxide integrated metasurfaces with switchable functionalities at terahertz frequencies," *Adv. Opt. Mater.*, vol. 6, no. 9, May 2018, Art. no. 1701204.
- [55] X. Li *et al.*, "Switchable multifunctional terahertz metasurfaces employing vanadium dioxide," *Sci. Rep.*, vol. 9, no. 1, Apr. 2019, Art. no. 5454.